Geophysical Journal International

Geophys. J. Int. (2019) **216,** 319–331
Advance Access publication 2018 October 05
GJI Seismology

doi: 10.1093/gji/ggy414

A model for nonlinear elasticity in rocks based on friction of internal interfaces and contact aging

Christoph Sens-Schönfelder[1], Roel Snieder[2] and Xun Li[2]

[1] *GFZ German Research Centre for Geosciences, Potsdam 14473, Germany. E-mail: sens-schoenfelder@gfz-potsdam.de*
[2] *Center for Wave Phenomena, Colorado School of Mines, Golden, CO 80401, USA*

Accepted 2018 October 4. Received 2018 September 23; in original form 2018 June 7

SUMMARY

Non-classical nonlinear elasticity in micro-inhomogeneous materials such as rocks and cracked or granular materials leads to a number of phenomena ranging from hysteresis and memory to a transient response of elastic properties to perturbations in dynamic or quasi-static experiments. Dynamic acousto-elastic testing (DAET) provides very detailed observations of some of these phenomena that are still not fully understood in terms of their physical origin. We suggest that the observations of non-classical nonlinear elasticity can be related to the physics of friction. We propose a conceptual model for the nonlinear elasticity based on friction of internal interfaces and the process of contact aging that leads to an increase of friction with increasing contact time. The central element of the model is the continuous interplay between (1) softening that occurs as small-scale damage due to shear motion of internal contacts and (2) stiffening (healing) as a thermally activated process of establishing connections across the contact at the current strain state. Chemical bonds, mineral fibres or capillary bridges are the most likely candidates for the physical nature of these connections. Our model qualitatively describes dynamic softening, hysteresis, slow dynamics and the shape of DAET loops including the absence of cusps and the loop orientation that leads to a stiffening at both maxima and minima of the dynamic strain.

Key words: Elasticity and anelasticity; Friction; Wave propagation; Acoustic properties; Rheology and friction of fault zones; Plasticity, diffusion, and creep.

1 INTRODUCTION

Micro-inhomogeneous materials such as rocks, granular material or damaged structures containing cracks exhibit non-classical nonlinear elasticity that originates in the change of material properties at cracks or grain boundaries caused by deformation or other disturbances (Guyer & Johnson 1999, 2009; Ostrovsky & Johnson 2001). Due to its origin on a spatial scale between the microscopic internal structure of grains and the macroscopic scale of observation, this property is often referred to as nonlinear mesoscopic elasticity (NME; Guyer & Johnson 1999, 2009). Compared to classical elastic nonlinearity caused by the anharmonic shape of the atomic potentials, NME has far stronger effects and a transient response that can be observed in static and dynamic experiments (Guyer & Johnson 2009).

A classic observation of NME comes from the measurement of the stress–strain relation in slowly performed load experiments. Quasi-static load experiments on cast iron were already performed by Berliner (1906) and showed hysteresis, endpoint memory and slow transient after-effects. Hysteresis introduces memory in the system since the stress depends not only on the strain but also on the strain history. Endpoint memory refers to the following property: if the material is moved along one curve in the stress–strain space, it will evolve along another curve when the loading is reversed at state (A) due to hysteresis. If now the loading is reversed again at state (B) the system will evolve along a third curve that will pass through the earlier endpoint at state (A) again and continue the initial curve as if the excursion $A \rightarrow B \rightarrow A$ had not happened. In geomaterials these properties were intensively studied, for example, by Guyer *et al.* (1995, 1997).

Resonant bar experiments were typically used to study the NME-response to dynamic excitations with fast cyclic variations of strain (Guyer *et al.* 1998; TenCate *et al.* 2000, 2004; Pasqualini *et al.* 2007). In these experiments, a rock bar is excited by longitudinal oscillations close to its resonance frequency which is determined by the amplitude peak during frequency sweeps across the resonance. NME leads to a nonlinear decrease of the resonance frequency with increasing amplitude of the excitation, a distinct response for upward- and downward-frequency sweeps (hysteresis) and a transient re-increase of the resonance frequency after termination of the high-amplitude excitation (Johnson *et al.* 1996; TenCate *et al.* 2000; Ostrovsky & Johnson 2001). The recovery process is often called *slow dynamics* (TenCate 2011) and refers to a linear increase of the elastic moduli on a logarithmic timescale. Similar observations

have been made using cross-modulation experiments that record the amplitude variations of a probe wave induced by a pump wave of higher amplitude and different frequency (Zaitsev *et al.* 2005). Waveform changes of a travelling wave due to NME were studied by Remillieux *et al.* (2017). The elastic nonlinearity of NME materials that is expressed by (1) coupling of wave propagation at different frequencies through cross-modulation, (2) excitation of harmonics, (3) decrease of the modulus and (4) increase of attenuation is sometimes termed *anomalous fast dynamics*. These phenomena have been shown to occur together with slow dynamics (Johnson & Sutin 2005).

The variation of the elastic moduli that underlies the change of the resonance frequency can also be observed with high accuracy as a change of the acoustic wave speed (Larose & Hall 2009; Tremblay *et al.* 2010). Such measurements that can be performed in seismology on a much larger scale (Sens-Schönfelder & Wegler 2011) show a decrease of the elastic moduli in near surface materials at the time of earthquake shaking and a post-seismic transient recovery over months to years (Brenguier *et al.* 2008; Hobiger *et al.* 2013; Gassenmeier *et al.* 2016).

Various models have been suggested for different aspects of NME. An early model for the hysteresis, endpoint memory and relaxation in load experiments was proposed by Prandtl (1928a). It relates the mentioned observations to the behaviour of chemical bonds across grain contacts that slide through a sinusoidal potential when the contact is sheared. Known as Prandtl–Tomlinson model (Tomlinson 1929; Popov 2010), it is now frequently used in the physics of friction. To reproduce the endpoint memory, Prandtl (1928a) assumes that a number of such sliding interfaces with a range of amplitudes of the sinusoidal potentials is present in the material.

A review of early models of the nonlinear acoustic behaviour of rocks is included in Ostrovsky & Johnson (2001). The classical approach to the description of elastic nonlinearity is the extension of the stress–strain relation to higher orders in strain (Landau *et al.* 1986). This accounts for atomic nonlinearity, but it fails to account for the time dependence and hysteresis observed in NME. A phenomenological model for the hysteresis and endpoint memory in quasi-static experiments is the Preisach–Mayergoyz (PM) space (Guyer *et al.* 1995, 1997) that uses a set of bistable hysteretic elements that flip at different stress levels back and forth between two states with different contribution to the material's modulus. Due to the lack of a relaxation mechanism the PM-space model fails to reproduce slow dynamics. This has been fixed by including Arrhenius-type transition probabilities between the states in the PM space (Gusev & Tournat 2005). The hysteretic elements of the PM space have been used in to model wave propagation by Delsanto & Scalerandi (2003) and Vanaverbeke & Abeele (2007).

Lyakhovsky *et al.* (1997) presented a damage rheology model for load experiments that did not focus on acoustic observations at small strains but leads to interesting results. The model uses a single damage state parameter that affects the elastic moduli of the damaged material. The kinetics of the damage parameter is based on thermodynamic principles and leads to regimes of healing and fracturing depending on the strain invariant ratio. A damage parameter that scales the tension–compression asymmetry of the stress–strain relation in a cracked medium was used by Lyakhovsky *et al.* (2009) to describe quasi-static observations as well as the decrease of the resonance frequency with increasing drive amplitude in dynamic experiments.

Vakhnenko *et al.* (2006) presented the soft ratchet model for longitudinal vibrations in a rock bar. The model uses the interaction between a fast and a slow subsystem, where the fast system is responsible for the wave propagation and the slow subsystem represents the response of the cohesive bond system to the deformation. The bonds break and are re-established at different rates that depend on the applied stress. The soft ratchet model involves a number of timescales for breaking and reforming the bonds. Vakhnenko *et al.* (2006) arrive at a comprehensive description of NME including the shape of resonance curves and the amplitude-dependent frequency shift, that is, softening.

Zaitsev *et al.* (2014) assume adhesive Hertzian contacts that can exist in open and closed configurations depending on the distance of the surfaces of soft contacts. A range of energy barriers between the two states of these bistable contacts is required to reproduce the correct dynamics. However, the model assumes tensile shocks as excitation and it does not predict the response to symmetric perturbations.

A physical connection between hysteretic elements and adhesive asperities in rough contacts under longitudinal deformation was proposed in a model by Aleshin & Van Den Abeele (2005, 2007) . The distribution of forces for closing and opening the adhesive asperities results from a range of curvatures in the rough contact surfaces. Aleshin & Van Den Abeele (2007) show that the stress–strain curves in quasi-static load experiments as well as the resonance frequency shift in resonant bar experiments could result from the adhesion forces on the micro/nanoscopic scale of individual asperities.

Lieou *et al.* (2017) modelled the material softening observed in granular material as the number of 'shear transformation zones', which represent soft spots in the medium. The number of these soft spots, which reflect locations of strain concentrations depends on the dynamic strain amplitude and correlates with the modulus reduction. This model can account for the modulus reduction with increasing dynamic excitation but does not explain the time dependency of healing.

In Li *et al.* (2018), we presented a model for hysteresis and bifurcation in resonance experiments that takes into account the feedback of dynamic softening on the excitation amplitude. This model is based on the variable thermodynamic equilibrium of a bistable system in an energy landscape that is perturbed by normal strain. It does not consider shear deformation and is unable to reproduce some of the observations in dynamic acousto-elastic testing (DAET) experiments that will be discussed in Section 1.1.

In summary, this limited overview of existing models for NME shows that some models depend on longitudinal excitation and others on shear excitation. But all models are based on bistable structures with different contributions to the elastic moduli and strain-dependent transition probabilities. Often a range of energy barriers for the transitions is used to describe the transient response of NME which is a simple mechanism for the $\log(t)$ recovery in slow dynamics (Snieder *et al.* 2017). It indicates that a number of processes with different characteristic times are active during the recovery period.

Of particular value for the investigation of dynamic softening are DAET experiments, that are similar to a resonant bar experiment with the additional possibility to track the modulus of the material *during* each cycle of the strain (Renaud *et al.* 2012). While the traditional set-up measures the resonance frequency and thereby averages over the changing properties during several strain cycles, DAET can resolve the dynamics of the elastic properties during the change from compression over maximum strain rate to dilation and back. This makes it possible to separate processes depending

on their timescale. Fast processes instantaneously adapt to changing conditions while slow processes do not respond to the changes within a cycle. The observed dynamics, therefore, reflects predominantly the processes with timescales equal to the inverse of the excitation frequency. This provides valuable information about the physics of the individual processes that is otherwise hidden in their collective response observed with resonant bar or quasi-static load experiments.

In this manuscript, we show that DAET observations suggest an important role of shear deformation and friction in NME. We present a conceptional model to explain various observations of NME including DAET with frictional processes on internal interfaces such as cracks or grain boundaries.

1.1 DAET experiments

A series of DAET experiments investigated the detailed nonlinear behaviour of different rocks (Renaud *et al.* 2012, 2013; Rivière *et al.* 2013, 2015). Longitudinal, shear (Lott *et al.* 2017) and complex flexural deformation from impacts (Eiras *et al.* 2016) have been used as excitation. The response of a single fatigue crack was investigated (Rivière *et al.* 2014) as well as the *in situ* nonlinearity of soil on the scale of metres using seismic equipment and a vibrator truck (Renaud *et al.* 2014). Rivière *et al.* (2016) studied the frequency, pressure and strain dependency of the nonlinear response. Finally, the spectrum of recovery times for a number of materials was measured by Shokouhi *et al.* (2017). DAET experiments are performed with a pump and a probe wave of a certain wave type and polarization. This allows to investigate the complex anisotropic response of the material as a function of propagation directions and polarizations of the two participating waves (Lott *et al.* 2017). A variant of the typical DAET set-up that measures the response during steady-state oscillation of a standing wave was used by TenCate *et al.* (2016). In their set-up, two travelling waves are sent through the sample in perpendicular directions and the time delay of the small-amplitude probe wave is measured at different phases of the perturbing pump wave. With this approach TenCate *et al.* (2016) could infer variations in the nonlinear response depending on the propagation directions with respect to the symmetry axis of an anisotropic sample.

For the following discussion, it is essential to understand the principle of the DAET experiments that separate the perturbation process induced by a low-frequency pump wave (up to several kilohertz) from the observation typically performed with a low-amplitude ultrasonic pulse of MHz frequency. While the low-frequency pump oscillation is longitudinal along the rock bar, the probe wave is transmitted across the bar perpendicular to the pump oscillation to sense a well-defined state of the spatially varying strain. The main observation of DAET is the velocity of the probe wave as function of time, or alternatively as function of the pump strain during steady-state oscillation. For easy comparison of our model with the experimental observations, we reproduce the relevant figure from Renaud *et al.* (2013) in Fig. 1.

Each of the loops in Fig. 1 was measured by Renaud *et al.* (2013) in a different experiment during steady-state oscillation with a peak pump strain indicated by the horizontal extent of the loops. The excitation frequency was 4.5 kHz in all cases. We do not intend to model these loops in quantitative detail but present a model that is able to reproduce the main features of the observations in Fig. 1. These are (1) decrease of the average modulus of the loops for increasing peak amplitude of the pump strain, (2) existence of hysteresis, (3) absence of cusps at the strain maxima (4) orientation of the loops with increasing modulus at both positive and negative peak strain, (5) generally higher modulus at lower strain and (6) transition of the shape from sloping loops at large-peak strain to parabolic shapes at small strains. As we will see, the observations (5) and (6) can be modelled as functions of the strain. The main focus here is on observations (1)–(4) that are neither functions of strain nor strain rate and involve some more complex process. Additional to the properties of the DAET loops, the slow dynamic recovery of the modulus is a standard observation that should result from the model.

Attempts to model the nonlinear signatures of DAET experiments were published by Gliozzi & Scalerandi (2014), Pecorari (2015), Trarieux *et al.* (2014) and Favrie *et al.* (2015). Gliozzi & Scalerandi (2014) perform a wavefield simulation in a 2-D medium that includes hysteretic elements similar to the PM space. While this model reproduces the dynamic softening, it does not reproduce the shape of the loops including the orientation with increasing modulus at maximum absolute strain. The model of Pecorari (2015), which is based on the interaction of dislocations with point defects and microcracks, reproduces the softening and the shape and orientation of the DAET signatures reasonably well but exhibits a discontinuity of the modulus at zero strain and does not reproduce the healing.

Trarieux *et al.* (2014) used a third-order expansion of the complex elastic modulus to explain the nonlinear signatures of water, silicon oil and water saturated glass beads. They are able to reproduce the observed hysteresis, and tension–compression asymmetry also of hollow air-filled glass beads that behave strongly nonlinearly similar to rocks. Even though this approach is useful to quantify the nonlinear behaviour, it does not provide insight into the physics and it fails to reproduce the dynamic softening as a significant component of the mesoscopic nonlinearity expressed by the overall drop of the velocity in response to dynamic excitation. A numerical scheme for 1-D wave propagation is developed by Favrie *et al.* (2015) that combines the soft ratchet model (Vakhnenko *et al.* 2006) for creation and destruction of defects with a nonlinear extension of Hook's law and viscoelasticity to model fast and slow dynamic effects. Even though the authors obtain some qualitative agreement with DAET observations, their model shows only very small amount of softening (slow dynamics) in the presence of strong-fast nonlinearity reflected by large modulus changes. Also, it is not clear whether the orientation of DAET loops is correctly reproduced. An overview of models that attempt to describe the nonlinear elasticity and its relation to damage is given by Broda *et al.* (2014).

2 SHEARED CONTACT MODEL FOR NONLINEAR ELASTICITY

Examination of the patterns in the DAET signatures in Fig. 1 leads us to identify three independent components of the nonlinear response. We first note that the DAET signatures in Fig. 1 can be separated into the difference between the branches of increasing and decreasing strain on the one hand and their average on the other hand.

The average signal can be modelled with simple functions of the axial strain amplitude ε that we assume to be representative for the average compressional strain on the ensemble of contacts on the one hand and the average shear strain on the other hand. We assume here that the shear strain averaged over the ensemble of randomly oriented internal contacts can be represented by the absolute value of the axial strain $|\varepsilon|$. The average of the increasing and decreasing branches of the DAET signals is then composed of a linear trend

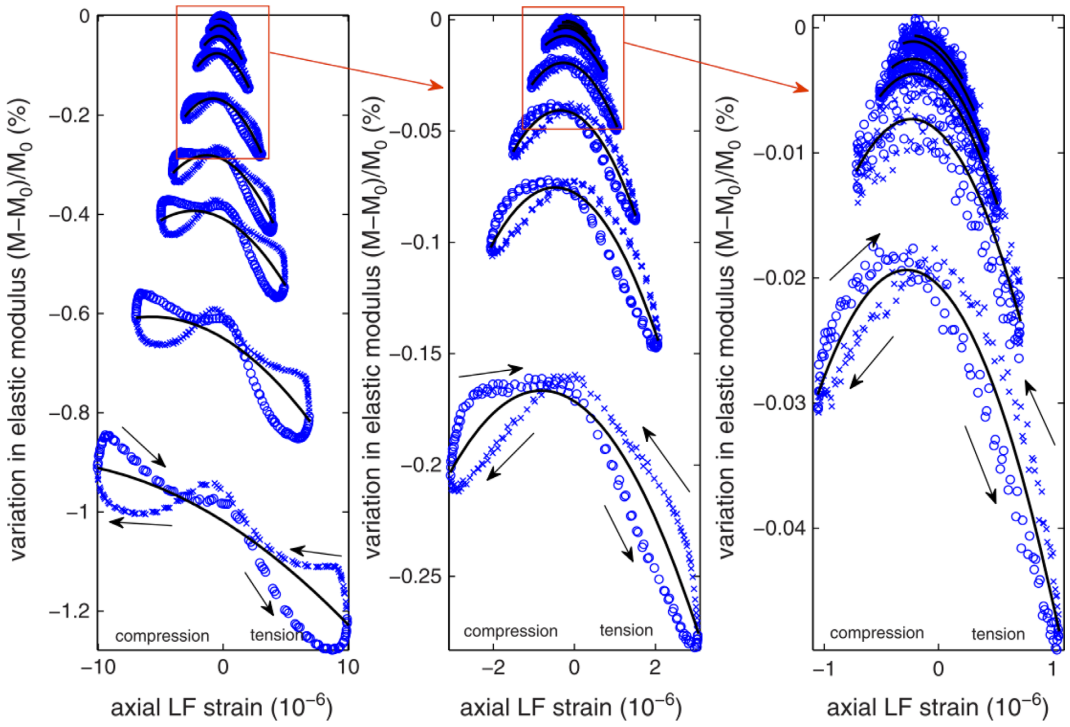

Figure 1. Variation of the elastic modulus of Berea sandstone during a cycle of the pump wave (from Renaud *et al.* 2013). The different closed curves correspond to different experiments with different pump amplitudes.

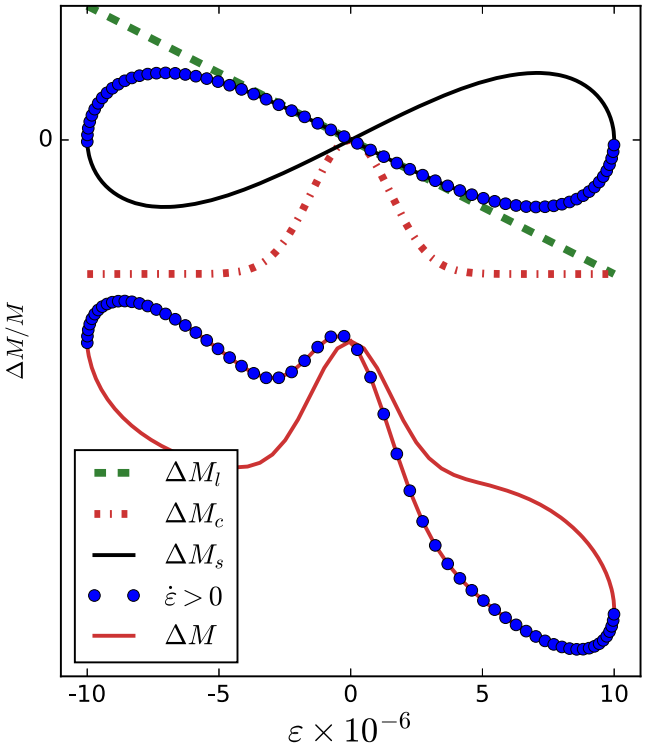

Figure 2. Schematic illustration of the components of DAET signatures. ΔM is the combined effect with an additional offset of the mean modulus.

(green dashed line marked ΔM_l in Fig. 2) of decreasing modulus for increasing strain (tension) and an approximately Gaussian contribution of fixed width with a parabolic maximum in the centre that flattens out towards large strain (red dash-dotted line marked ΔM_c in Fig. 2). Low-strain experiments sense its central parabolic part that causes a high modulus at smallest absolute strain. Large-amplitude experiments sense the whole shape of the Gaussian which causes a bump centred at the unstrained situation.

The difference signal (hysteresis of the loops in Fig. 1) is more complicated. It is neither a simple function of strain nor of strain rate. Empirically it approximately resembles a bow tie shape illustrated in Fig. 2 with the ΔM_s curve in black. There is a strong increase of modulus at maximum absolute value of strain and a decrease of modulus across the central part of vanishing strain. Important is the orientation of the bow tie loop indicated by the blue dots that mark the branch of increasing strain. The resulting modulus of the material that is perturbed by the different effects reads

$$M = M_0 + \Delta M_\mathrm{l} + \Delta M_\mathrm{c} + \Delta M_\mathrm{s} \tag{1}$$

and is illustrated in Fig. 2.

Additional to these components that model the shape of the nonlinear signatures, there is a shift of the whole signature towards smaller modulus with increasing amplitude of the pump strain. This overall modulus decrease and the recovery result as a natural consequence of the process that we suggest to model the bow tie shaped signal component ΔM_s. In the following, we describe the mathematical form and physical explanations of these three modulus perturbations.

We linearize the decrease of modulus with the strain in the DAET signatures and thus account for it by a linear function

$$\Delta M_\mathrm{l}(t) = -A\varepsilon(t). \tag{2}$$

This linear dependence describes the well-known increase of the modulus under compression (King & Paulsson 1981). In addition, we add the following dependence of the modulus on the strain:

$$\Delta M_\mathrm{c}(t) = B\left(\exp\left[\frac{-\varepsilon(t)^2}{2w^2}\right] - 1\right). \tag{3}$$

This component of the modulus shapes its behaviour in the central part of the deformation curve for strain with absolute value less than the width w. We propose that it results from shear motion on the rough interface of a crack. Shear motion occurs in a rock sample due to internal heterogeneity and the intrinsic shear deformation in any elastic wave even if the macroscopic excitation is longitudinal. In this situation, it is reasonable to assume that the roughness is random but to some extent correlated on both sides of the crack for zero strain. In the unstrained situation the surfaces fit into each other like two puzzle pieces, maximizing the contact area and consequently the modulus. If the crack is sheared the fit is less good and the contact area decreases due to the progressive mismatch until it is finally restricted to the tips of the surfaces leading to a decreased modulus (Borri-Brunetto *et al.* 2001). For larger shear, beyond the correlation length of the surface roughness, the two sides of the crack are uncorrelated and the average contact area does not depend on the strain any more.

Hysteresis, decrease of average modulus, the orientation of the DAET loops and slow dynamic recovery are all contained in ΔM_s which is the main focus of this article. We suggest that ΔM_s is a consequence of friction on internal interfaces in heterogeneous materials.

We propose to model the contribution of the frictional interfaces to the macroscopic modulus as the number of broken connections across an interface normalized for the total number of potential connections:

$$\Delta M_s(t) = -CN(t)\,. \tag{4}$$

This is motivated by friction models (Prandtl ; Capozza & Urbakh 2012; Capozza *et al.* 2013; Li *et al.* 2014), observations of single asperity friction (Li *et al.* 2011) and the fact that heterogeneous materials such as rocks contain a myriad of contacts with a range of sizes and loading conditions of which some contacts experience tangential deformation in the macroscopically longitudinal strain field. These connections can be established as capillary bridges (Bocquet *et al.* 1998; Barel *et al.* 2012), chemical bonds or van der Waals forces (Li *et al.* 2011; Liu & Szlufarska 2012; Tian *et al.* 2017) or adhesive contacts (Aleshin & Van Den Abeele 2007; Barthel 2008). Even fibres of minerals that grow in cracks as observed *in situ* by Vanorio (2015), Hilloulin *et al.* (2016), Wiktor & Jonkers (2011) and Vanorio & Kanitpanyacharoen (2015) could establish such connections. All these types of connections are thermally created and destroyed when the connections are deformed. The number of existing connections results from the two competing processes of constantly forming new connections and connection breaking when the material is deformed.

We denote the fraction of broken connections by N_i. The subscript i indicates that there is a multitude of microstructures that heal at different rates. For the processes of creation of connections we assume a simple exponential form with a characteristic time τ_i, where the rate at which connections are established is N_i/τ_i. Connections break when the medium is deformed, and they break at a higher rate when the medium is deformed faster—leading to a dependence on strain *rate* rather than strain. This can also be explained in terms of the mean lifetime of connections that decreases with the rate of displacement. Moreover, the sign of the strain rate is irrelevant for the shear motion that strains the connections and we approximate the rate at which connections break with linear function of the absolute value of the strain rate and the number of established connections. This leads to the following differential equation for the fraction of broken connections N_i:

$$\frac{\mathrm{d}N_i}{\mathrm{d}t} = \frac{\nu|\dot{\varepsilon}|}{\tau_i}(1 - N_i) - \frac{1}{\tau_i}N_i\,. \tag{5}$$

N_i varies between 0 indicating the perfectly relaxed state when all possible connections are formed and 1 when all connections of type i are broken. In eq. (5), the second term involving $-\tau_i^{-1}N_i$ accounts for the healing over a time τ_i. The term $\nu|\dot{\varepsilon}|\tau_i^{-1}(1 - N_i)$ describes excitation (breaking) of connections. This rate is proportional to the fraction $(1 - N_i)$ of existing connections, as well as the strain rate $|\dot{\varepsilon}|$ meaning that no structures are damaged when the medium is at rest ($\dot{\varepsilon} = 0$). In this case, the second term leads to exponential recovery with time τ_i. The strain rate and the constant ν normalize the characteristic time τ_i for the destruction of connections. ν describes the susceptibility of the material's elastic constants to dynamic deformation. It is the inverse of a characteristic strain rate at which damage becomes more effective than healing. It has a similar meaning as the susceptibility used by Brenguier *et al.* (2014). The strain rate dependence is likely more complicated than suggested by the linear function, which we choose for simplicity. We note that the equilibrium number of broken connections approached for constant $|\dot{\varepsilon}|$ is independent of i, namely $N_{\mathrm{eq}} = \nu|\dot{\varepsilon}|/(1 + \nu|\dot{\varepsilon}|)$. This form is closely related to the hyperbolic model for the shear modulus of soil under cyclic loading used in earthquake engineering (Duncan & Chang 1970; Hardin & Drnevich 1972). The average number density of damaged connection is given by

$$N = \frac{\sum_i \frac{1}{\tau_i} N_i}{\sum_i \frac{1}{\tau_i}}, \tag{6}$$

where the pre-factor $1/\tau_i$ increases the weight of fast processes required by the $\log(t)$-recovery during the slow dynamics process (Snieder *et al.* 2017).

3 NUMERICAL EXPERIMENTS

We demonstrate the ability of the sheared contact model to qualitatively reproduce available observations in three numerical experiments. Like the experiments that were performed by different groups using different samples and set-ups our numerical experiments simulate different situations expressed in different parameters.

3.1 DAET signatures

Using eqs (1)–(6), we model the response of the material to harmonic excitations of different amplitudes. The parameters used for this experiment are given in column Exp. 1 of Table 1. Fig. 3 shows the time-series of the resulting modulus for an experiment analogous to Renaud *et al.* (2013), where the sample is perturbed with a sinusoidal pump wave with a frequency of 4.5 kHz and a peak strain of 10^{-6}.

The modulus shows the same behaviour as in the experiments of Renaud *et al.* (2013). During the action of the pump wave the modulus fluctuates around a short-term mean that decreases rapidly in the beginning and slowly converges towards a lower value. When the excitation stops at 0.31 s the modulus re-increases—very fast in the beginning and slower at later times.

Interesting detail about the processes that cause changes of the modulus is revealed by the short-term response of the modulus captured in the nonlinear signatures during DAET. Following the procedure of Renaud *et al.* (2013), we model the signatures shown in Fig. 4. Curves corresponding to increasing strain are plotted blue.

Table 1. Model parameters used for the simulation of the nonlinear behaviour. ' ~ ' indicates that the value is identical to the previous experiment listed to the left.

Symbol	Meaning	Exp. 1	Exp. 2	Exp. 3
A	Slope of linear component	$160\,M_0$	~	0
B	Amplitude of central component	$0.002\,M_0$	0	0
w	Width of central peak	1.5×10^{-6}	~	~
C	Amplitude of strain rate-dependent change	M_0	~	~
ν	Damage susceptibility	0.08 s	8 s	1000 s
$\tau_{\min}$	Shortest timescale of healing	1×10^{-5} s	~	0.01 s
$\tau_{\max}$	Longest timescale of healing	100 s	~	~

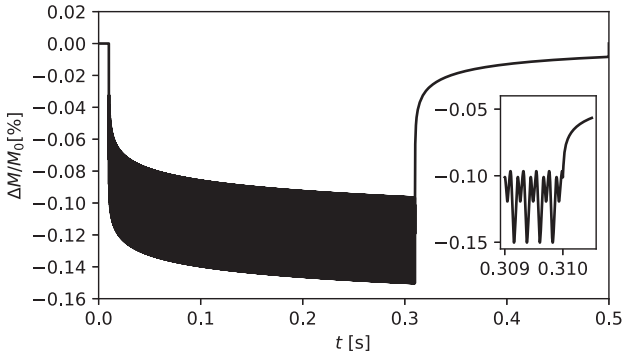

Figure 3. Modelled perturbation of the elastic modulus due to a 4.5 kHz sinusoidal strain excitation of 10^{-6} from 0.01 s to 0.31 s. The appearance of the curve as a thick line results from the high-frequency fluctuations during the action of the pump shown in the close-up around 0.31 s when the pump is turned off.

The bottom curve in the rightmost panel corresponds to the time-series shown in Fig. 3 around 0.3 s. These modelling results are to be compared with the experimental observations reproduced in Fig. 1. Qualitatively the signatures reproduce the main features of the experimental observations listed in Section 1.1, which are most importantly the decrease of mean modulus with increasing peak strain, the existence of hysteresis and the orientation of the loops.

We quantify the shape of the signatures following Renaud *et al.* (2013) by approximating them with second-order polynomials. The approximations are indicated in green in Fig. 4. In comparison to the observations by Renaud *et al.* (2013), Fig. 5 shows the parameters of these polynomials as function of maximum pump strain. Note that the figure displays the logarithm of the negative values. The average slope of the modelled signatures is constant at −160 as determined by the parameter A (Table 1) while it slightly decreases from −80 to about −160 for strain above 10^{-6} in the experimental data. The curvature of the signatures is approximately constant at -2×10^8 below 10^{-6} strain in model and experiment and then increases by about two orders of magnitude for larger strain. For the smallest strain, the estimated curvature of the modelled signature is slightly positive and does not plot in these axes. The decrease of the mean modulus expressed by the parameter C_E changes approximately linear in the logarithmic axis from 2×10^{-5} to 10^{-2} in the experiment while it covers the range from 10^{-4} to 10^{-2} in the model.

3.2 Frequency dependence

The time dependence of the damage and healing processes leads to a dependence of the response on excitation frequency. To compare our model predictions to laboratory measurements we conduct numerical experiments analogous to Rivière *et al.* (2016) in the frequency range from 0.2 to 200 Hz. In this second experiment, we use the parameters given in column Exp. 2 of Table 1 with the difference to Exp. 1 being the neglect of ΔM_c ($B = 0$) that is not observed by Rivière *et al.* (2016) and a larger damage susceptibility ν. To obtain results that can be compared to the observations of Rivière *et al.* (2016) we decompose the waveforms during the stationary phase of the oscillation into their harmonic components. We thereby obtain the spectral amplitudes of the velocity signal at the excitation frequency f_1 and its overtones $f_2 \ldots f_7$. Additionally there is the overall decrease of the average modulus indicated as f_0. This procedure is repeated with constant strain amplitude for various excitation frequencies and we plot the amplitudes of the harmonic components as function of frequency in Fig. 6.

Compared with the laboratory observations of Rivière *et al.* (2016) the numerical experiment reproduces the first-order behaviour. Except for the fundamental frequency component f_1 that does not show any frequency dependence, the amplitudes of all other components increase linearly with logarithm of frequency. The amplitude of the mean velocity decrease (f_0) is largest followed by the even overtones with decreasing amplitudes for increasing order of the overtone. Amplitudes of the odd overtones (f_3, f_5 and f_7) are at least an order of magnitude below the even harmonics and are not shown in Rivière *et al.* (2016). Absolute amplitudes differ from the experimental observations and could be adjusted with the model parameters A and C.

3.3 Slow dynamics

To illustrate how our model reproduces the typical observations of slow dynamic recovery we perform a third numerical experiment. Since this experiment focuses on the evolution of the mean modulus, we use an excitation that avoids fast oscillations as seen in Fig. 3 during the action of the pump. We achieve this by using a pump waveform that keeps the damage term in eq. (5) constant, that is, by using a triangular waveform with $|\dot{\varepsilon}| = \text{const}$ as indicated in the inset of Fig. 7(a). We also set parameters A and B to zero as ΔM_l and ΔM_c do only cause fast oscillations and do not contribute to the long term dynamics. Other parameters of Exp. 3 given in Table 1 are adopted to reproduce the long-term behaviour in analogy to TenCate *et al.* (2000) and Shokouhi *et al.* (2017). The excitation lasts for 80 s and the recovery is followed for 500 s. To illustrate the effect of the minimum timescale we use a minimum relaxation time $\tau_{\min} = 0.01$ s that matches the onset of the roughly linear regime observed by Shokouhi *et al.* (2017). The saturation of the damage phase can be observed because we use a much higher damage susceptibility of $\nu = 1000$ here. Fig. 7(a) shows the time dependence of the modulus as a function of the linear timescale. Red part shows the damaging phase during the action of the pump. The recovery process is shown with a black line. Figs 7(b) and (c) show the damage and recovery phases on logarithmic time axis, respectively with t_0 and t_1 being the start and end times of the excitation, respectively. The minimum

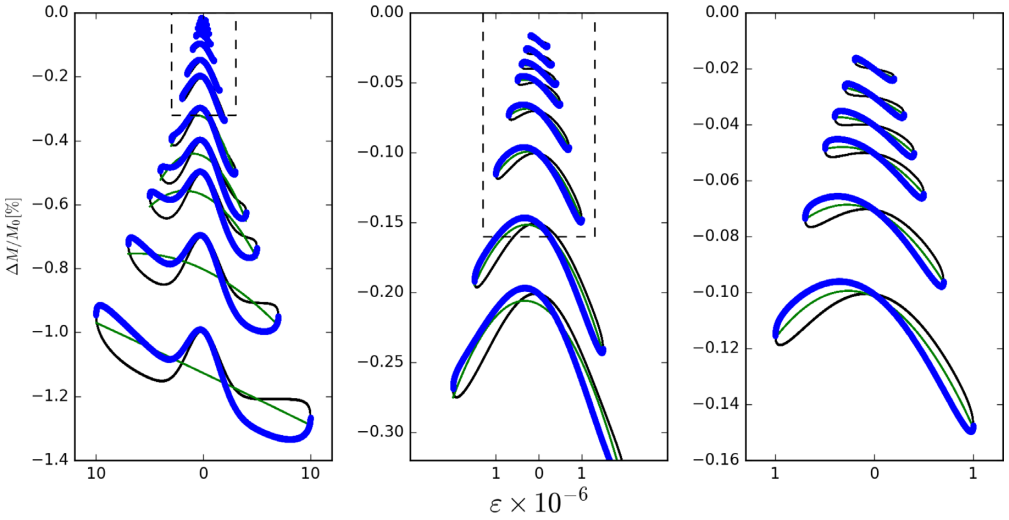

Figure 4. Modelled nonlinear signatures for a range of strain amplitudes between 2×10^{-7} (top in right-hand side panel) and 10^{-5} (bottom in left-hand side panel). The segments of increasing strain are plotted blue. Dashed boxes indicate the regions enlarged in the plot to the right. Green curves indicate second-order polynomial fits of the signatures to quantify the shapes (Fig. 5).

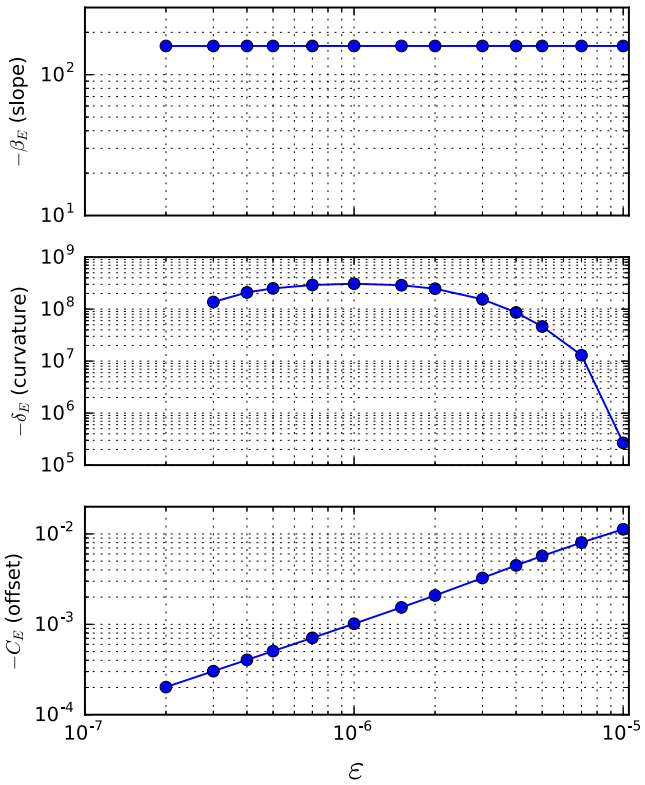

Figure 5. Amplitude dependence of the nonlinear signatures. C_E, β_E and δ_E are the coefficients of polynomial approximations of the signatures.

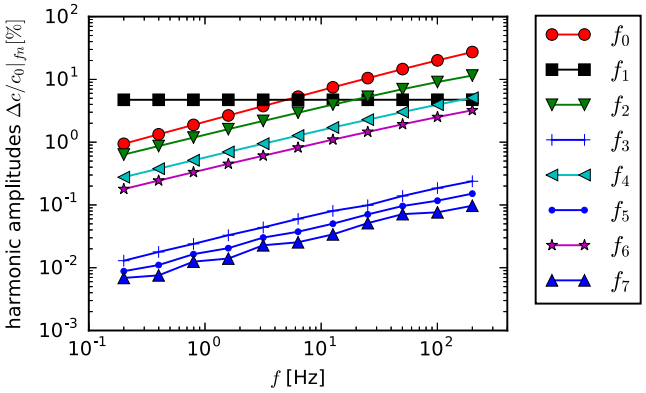

Figure 6. Frequency dependence of the nonlinear response as amplitude of harmonic signal components for constant strain amplitude.

and maximum timescales of the recovery process are indicated in Fig. 7(c). In Fig. 7(b), we indicate the end of the damage phase that occurs at $\tau_d = \tau_{max}/(1 + |\dot{\varepsilon}|\nu) = 5.3$ s for $|\dot{\varepsilon}| = 0.018$ s^{-1} of the triangular excitation used in this simulation. Change of the modulus during conditioning (approximately) and relaxation is linear on the logarithmic timescales similar to observations by TenCate *et al.* (2000) and Johnson & Sutin (2005). As in the examples of Snieder *et al.* (2017), the logarithmic time behaviour occurs for times $\tau_{min} < t - t_1 < \tau_{max}$. Deviations from linear recovery on a logarithmic timescale as observed by Shokouhi *et al.* (2017) could be included in the model using weights different from $1/\tau_i$ currently used in eq. (6).

4 DISCUSSION

4.1 Model parameters

The sheared contact model involves a number of parameters (seven) and it is able to reproduce a number of versatile observations:

(1) pressure dependence of velocity (linear strain dependence contained in ΔM_l),
(2) change of DAET loops shapes from bow tie shaped with a central bump at higher amplitudes to parabolic loops at smaller strain levels,
(3) bow tie shape of DAET loops and variation with amplitude,
(4) absence of cusps,
(5) existence of hysteresis in DAET loops,
(6) orientation of DAET loops,
(7) decrease of mean modulus with increasing dynamic excitation,

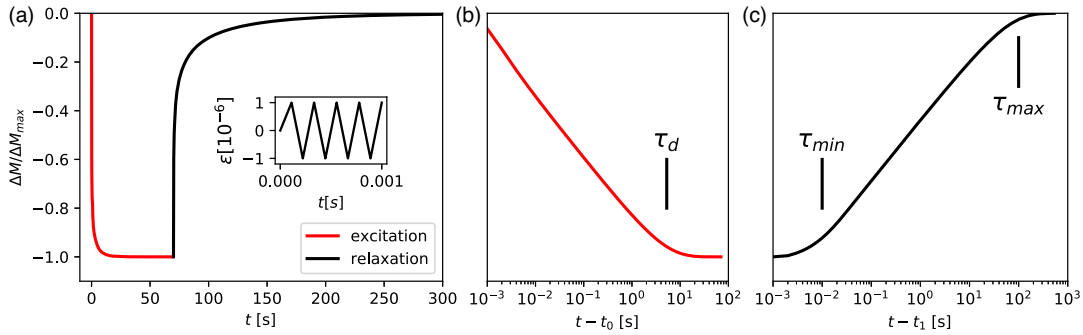

Figure 7. Slow dynamics of the damaging and relaxation phases. Modulus change during the damage phase is indicated in red while relaxation is plotted black. (a) Modulus change during experiment 3 on a linear time axis. Inset shows the triangular strain curve of the pump used to avoid oscillations. (b and c) show the damage and relaxations phases, respectively, on logarithmic time axes with t_0 being the start and t_1 the end times of the excitation, respectively. $\tau_{\min}$ and $\tau_{\max}$ in (c) indicate the range of relaxation times in this numerical experiment.

(8) slow dynamics with faster excitation than recovery and linear recovery on logarithmic timescale,

(9) constant f_1 component for variable frequency,

(10) linear decrease of mean modulus with logarithm of frequency,

(11) linear increase of overtone amplitudes with logarithm of frequency and

(12) amplitude difference between even and odd overtones.

It is interesting to realize which of these observations are related to which parameters. Observations (1) and (9) are directly related to strain contained in ΔM_l and are simply described by parameter A (eq. 2). Observation (2) is modelled by ΔM_c (eq. 3 with the two parameters B and w).

All remaining observations are related to ΔM_s that is intended to model the friction of internal contacts, which alters the number of connections across the interfaces in the bond system. It contains the time dependence of the response that is characteristic for the non-classical behaviour of NME. Apart from its amplitude (C), ΔM_s does only depend on a single parameter, the damage susceptibility ν. The ability to explain the above-mentioned observations is thus not provided by careful tweaking of numerous parameters but by the model itself. It results from the simple assumption that friction of internal contacts in the material contributes to the stress transfer through the medium and that friction of these contacts increases with time and decreases upon displacement—a standard observation in the physics of friction. Friction is determined by the state of the interfaces. This state is described by the number of connections across the interface that are constantly created but broken by shear deformation. Our model suggests that this interplay between creation and destruction of connections is at the origin of NME. In all simulations, the fraction of broken connections remains small ($N_i \ll 1$) indicating that no saturation occurs.

The range of timescales ($\tau_{\min}$ and $\tau_{\max}$) governs the extent of the linear regime of the slow dynamic recovery and the excitation process. It has a minor influence on the shape of the DAET loops as long as $\tau_{\min} < 1/f_1 < \tau_{\max}$. Since the range of timescales is implemented explicitly to model the $\log(t)$ recovery, its occurrence itself is not a surprise. The important observation is that the model shows all the other desired properties of the DAET loops under the constraint that it also reproduces the slow dynamic recovery. As shown by Shokouhi *et al.* (2017), the spectrum of recovery times is not necessarily constant but can be variable if the recovery is not $\log(t)$.

The modulus perturbation ΔM_c is probably the most ad hoc part of our model which is solely included to model the varying shape of the DAET loops in Fig. 1 expressed by the decrease of curvature with increasing peak strain (Fig. 5). Though easily justified by the progressive mismatch during shear of correlated rough interfaces that reduces the contact area (Borri-Brunetto *et al.* 2001) it is not well supported by experiments. Moreover, this part of the modulus perturbation seems to be very variable between different materials (Rivière *et al.* 2015).

The linear perturbation ΔM_l with its parameter A is responsible for the constant slope of the signatures (Fig. 5) and the frequency-independent amplitude of the fundamental frequency component f_1 in Fig. 6. It is directly related to the stress sensitivity of the velocity (e.g. Shapiro 2003), which is related to the reduction of porosity expressed in Athy's law (Athy 1930). Since ΔM_l has different sign for compression and dilation, it must result from compression and it should thus disappear for shear excitation. This was indeed observed by Lott *et al.* (2017) as vanishing of the fundamental frequency component for shear excitation.

4.2 Frequency and pressure dependence of the nonlinearity

Our model qualitatively reproduces the experimentally observed frequency dependence by Rivière *et al.* (2016). The amplitude of the velocity variation at the frequency of excitation (f_1) is independent of frequency. Oscillations at f_2, f_4 and f_6 as well as the static offset (f_0) vary with frequency according to a power law $\Delta c/c = \Phi f^{\mu}$. The harmonics at three, five and seven times the excitation frequency have drastically lower amplitude compared to the even harmonics as observed in the experiment, but follow the same power law. The power-law exponent is $\mu \approx 0.5$ in our simulations compares to $\mu \approx 0.16$ found experimentally by Rivière *et al.* (2016). This difference might indicate that the damage and healing processes are not simply related to the strain rate but depend to some degree on strain itself. This could lower the frequency dependence.

The wave velocity depends on porosity ϕ as described by ΔM_l, which is a linearization of the exponential porosity-pressure dependence for small fluctuations: $\phi = \phi_0 \exp(-\theta \beta_s P)$. Here P is effective pressure, β_s is stiff compressibility, ϕ_0 is porosity at zero pressure and finally θ is the piezosensitivity (Shapiro 2003). However, the decreasing porosity with increasing pressure does not only increase the velocity, it also removes the weak parts of the bond system that are responsible for NME (Johnson & Sutin 2005). We

thus propose that the parameters A, B and C that scale the nonlinear components in our model all depend on the compliant porosity as described above. This coincides exactly with the functional form used by Rivière *et al.* (2016) to describe dependence of nonlinearity on confining pressure where the characteristic pressure P_0 of Rivière *et al.* (2016) equals $1/\theta\beta_s$ of Shapiro (2003).

4.3 Absence of cusps and the different moduli

The absence of cusps at maximum strain of the DAET measurements appears to be in contrast with the quasi-static observations of Guyer *et al.* (1997), Ostrovsky & Johnson (2001), TenCate (2011) and Rivière *et al.* (2016). How does our model reconcile these observations from quasi-static and dynamic experiments? A detailed modelling of the quasi-static experiments is beyond the scope of this paper, but we sketch the simple mechanism that explains both the fast DAET and the quasi-static experiments.

In quasi-static load experiments, hysteresis leads to the open curves in the stress–strain behaviour that follow different paths for increasing and decreasing strain. Since there is no possibility to measure the stress directly in DAET experiments, one uses the wave velocity of a probe wave to sense changes of the elastic modulus. Also the velocity follows open curves in the strain–modulus space. However, the instantaneous modulus M seen by the probe cannot be interpreted as the one that relates the macroscopic stress σ and strain ε. Given the orientation of the loops, such an interpretation would lead to negative dissipation when integrating the strain energy density $E = 1/2M\varepsilon^2$ over the DAET loop.

Our model offers a simple mechanism to reconcile the orientation of the loops and absence of cusps in dynamic measurements with the fact that energy is dissipated rather than released by the material. In Fig. 8, we show an illustration of the connections in one of the frictional contacts present in the bond system during half a deformation cycle of the pump wave.

If the contact is sheared, connections are strained and break while new ones are formed at the current deformation state (Fig. 8b). At peak strain of the harmonic deformation the material is at rest for a moment meaning that no connections are damaged but healing goes on. This leads to stiffening of the material around the peak strain (Fig. 8c). When the strain rate reverses the deformation damages connections, which leads to fewer connections in place when the material passes through the zero-strain state (Fig. 8d). The modulus that is measured by the high-frequency probe wave in a DAET experiment is proportional to the number of connections across the crack—no matter which portions of the surfaces they connect.

On the other hand, the contribution of a connection to the macroscopic stress involved in the pump wave depends on its restoring force which in turn depends on the strain state under which it was created. The connections in Figs 8(c) and (d) that bridge the crack perpendicularly do not contribute to the stress involved in the pump wave of a DAET experiment or the static stress in a load experiment as they do not contribute to the restoring force. But they contribute to the modulus seen by the probe wave because they counteract any additional deformation (e.g. the probe). Therefore, the modulus seen by the probe wave must not be confused with the modulus involved in the macroscopic deformation. The modulus observed with the probe wave in the DAET signatures is thus not suitable to draw conclusions on the energy dissipation of the pump oscillation. Since the connections are established at the current deformation state, the healing process does not increase the strain energy. However, connections break when strained. Whenever a connection breaks, strain energy is lost, likely as heat for small structures (Prandtl 1928a) or as damage-related radiation for macroscopic structures (Ben-Zion & Ampuero 2009). This mechanism provides a link between deformation, velocity reduction and attenuation of the low-frequency excitation.

Hysteresis is only related to processes with characteristic times of healing (τ_i) larger than the timescale at which changes are induced in the experiments. Faster processes adopt instantaneously (compared to the experimental timescale) to any new strain and do not contribute to hysteresis. Since the number of contributing processes decreases for slower experiments, the hysteresis in slowly performed load experiments vanishes, as observed by Claytor *et al.* (2009).

The proposed mechanism, that healing occurs by establishing connections across a contact at the current strain state, can also explain the absence of cusps in DAET and their presence in quasi-static load experiments. In load experiments, the observed stress corresponds to the applied strain as there is no distinction between excitation and observation. So naturally, at maximum strain the modulus does not increase in the healing phase because the connections are established at exactly this strain and do not increase the restoring force. Since the healing process does not alter the macroscopic modulus relating stress and strain in the load experiment there are cusps at the turning points of the load protocols. In contrast, the probe wave in a DAET experiment will not see cusps due to the increase of connection at peak strain.

4.4 Relation to other friction models

Since we model NME with processes that occur during sliding of internal interfaces, it is legitimate to ask why we do not apply an established model from the physics of friction (see Baumberger & Caroli 2006 for an excellent review). This has the following reasons. We are (1) not interested in the friction coefficient of the interfaces, which is the target of most friction models. Instead we aim at a description of the interface's ability to contribute to the probe wave propagation. This difference relates to the difference between the modulus of the macroscopic deformation and the modulus seen by the probe wave discussed in the previous section. (2) Standard models like rate-and-state friction (Marone 1998; Rice *et al.* 2001) are unable to model oscillatory slip as they diverge for zero velocity and require adaptations that are less well established (Woodhouse *et al.* 2015). (3) We aim to model kilohertz vibration that might involve the regime of fast sliding in which friction models are not well constrained by experiments (Woodhouse *et al.* 2015). And finally (4) our model can be described in a single equation and has the physical motivation of established or broken connections that has been used as ingredient of fiction models (Prandtl ; Baumberger & Caroli 2006; Popov 2010).

However, we can still make a simple connection to rate-and-state friction in analogy to the illustration in Fig. 8. Rate-and-state friction with Dieterich's aging law and Coulomb's law is described by the following equations:

$$\mu = \mu_0 + a \ln\left(\frac{v}{v_0}\right) + b \ln\left(\frac{\psi}{\psi_0}\right) \tag{7}$$

$$\frac{\mathrm{d}\psi}{\mathrm{d}t} = 1 - \frac{v\psi}{L}, \tag{8}$$

where μ is the friction coefficient, v is the sliding velocity, ψ is the state variable and L, a and b are constants. Applying this model to internal interfaces the friction coefficient describes the ability of

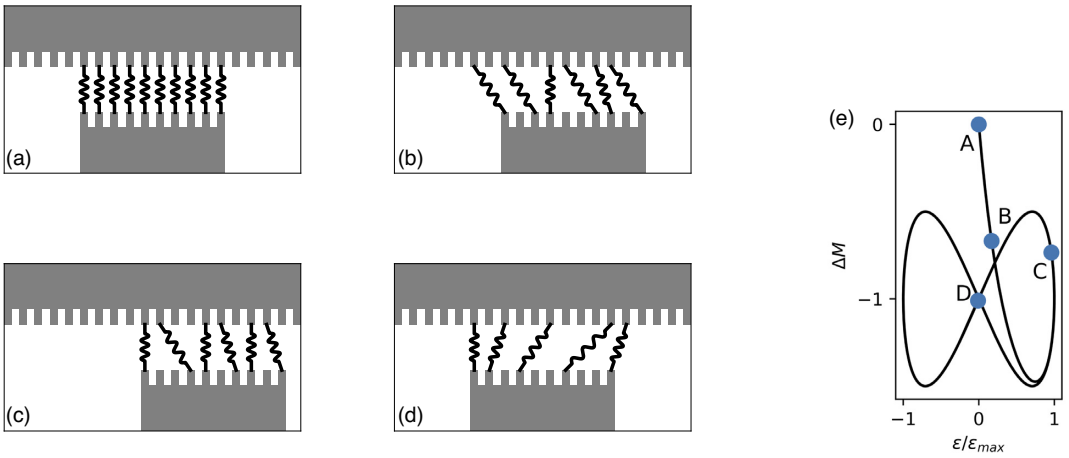

Figure 8. Illustration of contact with fragile connections formed by chemical bonds or capillary bridges. The contact is perfectly healed in (a) and deformed via (b) to peak strain illustrated in (c). When returning to the initial position the contact contains fewer connections (d). Locations of the states (a) through (d) in the DAET loops are illustrated in (e).

the interface to resist the shear stress and thus to contribute to the macroscopic elastic modulus. The second term involving the constant a diverges for $v = 0$. It describes the rate dependence of the shear strength and is important only for the macroscopic deformation. The third term involving b describes the influence of the state of the interface—its geometric age—and can be interpreted as the size of the real contact area (Baumberger & Caroli 2006) formed by the asperities of the rough interfaces (which are presumable rough even at the atomic scale; Mo *et al.* 2009). It is well established that the real contact area increases with the logarithm of contact time (Baumberger & Caroli 2006) just like the number connections in our model. We argue that the last term with its interpretation as real surface area could be used to describe the ability of the interface to transmit the additional stress perturbations of the probe wave. The evolution of the state term in Fig. 7 for oscillatory v indeed shows very similar characteristics to our model discussed above.

The two processes of aging and rejuvenation of contacts were directly observed by Li *et al.* (2011) due to the formation of bonds across a single silica asperity in an atomic force microscope. Frictional aging is discussed as a potential origin of rate-and-state friction and provides an explanation for velocity-dependent friction (Popov 2010). As healing in our model, the frictional aging exhibits $\log(t)$ dynamics (Frye & Marone 2002; Nagata *et al.* 2008; Li *et al.* 2011). In fact our model is similar to the model by Prandtl (1928a) for friction on internal interfaces as explanation for elastic hysteresis, after-effects and viscosity. The additional assumption in our model is that connections/bonds do not only hop to closer locations when a contact is sheared, they can also remain broken for some time before creating a connection to a new location.

Assuming that NME is indeed related to the frictional properties of internal interfaces as suggested by our model, we can draw on investigations of frictional interfaces to constrain the physical nature of the connections in our model. In the physics of friction, a contact between two solid bodies of nominally macroscopic sizes consists of numerous microscopic asperities at which the materials are in real contact (range of repulsive atomic interactions). These asperities form nanometric adhesive junctions in which the interactions occur on the atomic scale. As pointed out by Bureau *et al.* (2002) and Baumberger & Caroli (2006), the aging and rejuvenation dynamics is due to the processes in the nanometric junctions rather than the asperities on the microscopic scale. We thus suggest that the connections used in our model should be seen as analogous to individual chemical bonds in the junctions between asperities rather interacting asperities in a macroscopic contact.

4.5 Implications for larger scales

Since we propose to model NME observed in centimetre scale samples with DAET experiments with the number of nanoscale structures, it is not clear how this description might be applicable to larger time and space scales important, for example, in the observation of the coseismic decrease of seismic velocity (Wegler & Sens-Schönfelder 2007; Brenguier *et al.* 2008; Hobiger *et al.* 2013; Gassenmeier *et al.* 2016). For the small scales it is obvious that the processes observed in the lab do also occur *in situ*. They are just more difficult to observe in the field on the fast timescales (Renaud *et al.* 2014). For the large scales we suggest without further discussion that this question relates to the fact that rate-and-state frictions laws, developed for observations with laboratory samples, are successfully used for the modelling of earthquakes (Scholz 1998). Similarly results obtained from acoustic emissions (AEs) in centimetre size lab samples are successfully extrapolated to the scale of reservoirs and fault zones (Goebel *et al.* 2017). We speculate that the spectrum of energy and timescales in our model used to reproduce the abundant observations of $\log(t)$ slow dynamics is linked to the range of spatial scales that contribute to the observed dynamics. The longest timescales of the field observations of NME (e.g. Gassenmeier *et al.* 2016) might thus be related to the larger spatial scales available in the field.

5 CONCLUSIONS

Inspired by the wealth of information in the observations of DAET experiments we have developed a simple mathematical model to explain variations of the seismic velocity in response to dynamic perturbations. The model consists of a material that contains structures, which are broken by shear deformation and closed by some chemo-physical process with a range of characteristic timescales, which continuously stiffens the material. The important element is that the healing involves a range of timescales including the fast timescales of the kilohertz vibrations used in DAET. Healing that

occurs at non-zero strain freezes this strain state which lead to stress–strain hysteresis and creep.

The decrease of the modulus for the same excitation will be smaller when the material is already damaged because there is a finite number of connections only and broken connections cannot be damaged any further. The strongest change will always be observed in the best healed condition. The response of the material to a unit excitation does therefore depend on the state of the material, that is, the number of existing connections N. This consideration indicates a relation between the softening in NME and brittle fracture where the Kaiser effect (Lavrov 2003) describes the increase of AE activity in a sample once the applied stress exceeds the maximum previously experienced stress. In fact regarding the event of breaking connections as smallest scale fractures our model reproduces the Kaiser effect in two aspects. First, damage inhibits further damage. And second, the recreation of connections heals the damage on a range of timescales similar to the decay of the Kaiser effect that disappears over hours or days (Lavrov 2003). One can imagine a continuum of structural and temporal scales ranging from reversible chemical bonds with fast healing rates that rupture without detectable acoustic signals over tiny asperities that generate AE and heal on timescales known from the decay of the Kaiser effect to macroscopic fractures with large healing times that make these structures practically irreversible.

For seismological observations of the seismic velocity, that is, the mean modulus, without detailed DAET information, our description allows modelling the evolution of the seismic velocity for a series of excitations based on measurements of the strain rate by fitting eqs (5) and (6) to the data. This should make it possible to infer values for the parameters C, ν, $\tau_{\min}$ and $\tau_{\max}$, which constitute a new set of material parameters with physical interpretations for dynamic loading and the nonlinearity between weak and strong motion.

The strain rate effect ΔM_s and the linear stress-dependent perturbation ΔM_l are distinct components of our model. But both effects might consistently originate at the same type of structures. If longitudinal deformation is introduced in the contact illustrated in Fig. 8 then dilatation leads to destruction of connections while compression increases the number of connections. However, both effects depend on the availability of compliant porosity and we can expect that materials with high piezosensitivity do also exhibit higher sensitivity to dynamic deformation as observed by Richter *et al.* (2014). But additionally we should expect a dependence of the dynamic effect on the chemistry of the rock and the availability of water as observed in friction experiments (Frye & Marone 2002; Li *et al.* 2011).

Creation and destruction of connection in our model are small-scale damage and healing processes. We expect these processes to occur in the weak parts of the bond system, that is, in the compliant porosity which depends on the effective pressure. The damage and healing process is therefore strong near the Earth's surface where the confining pressure is low. Due to pore pressure counteracting the confining pressure in saturated materials, the damage and healing processes will also be relevant in reservoirs, volcanoes (Brenguier *et al.* 2014; Lesage *et al.* 2014) and subduction zones (Chaves & Schwartz 2016). It might be an important process for dynamic triggering of earthquakes (Hill *et al.* 1993; Brodsky & van der Elst 2014) or volcanic eruptions (Watt *et al.* 2009; Nishimura 2017) and the damage and healing process might be an important agent in the evolution of the aftershock activity.

The internal connections in our model can be interpreted as a contribution to cohesion. They can alter the strength of a material. We suggest that this is a potential origin of the long term increase of the landslide activity after large earthquakes (Marc *et al.* 2015).

ACKNOWLEDGEMENTS

We thank the editor and two anonymous reviewers for their thoughtful comments.

REFERENCES

Aleshin, V. & Van Den Abeele, K., 2005. Micro-potential model for stress-strain hysteresis of micro-cracked materials, *J. Mech. Phys. Solids,* **53**(4), 795–824.

Aleshin, V. & Van Den Abeele, K., 2007. Microcontact-based theory for acoustics in microdamaged materials, *J. Mech. Phys. Solids,* **55**(2), 366–390.

Athy, L.F., 1930. Density, porosity, and compaction of sedimentary rocks, *Am. Assoc. Petrol. Geol. Bull.,* **14**(1), 1–24.

Barel, I., Filippov, A.E. & Urbakh, M., 2012. Formation and rupture of capillary bridges in atomic scale friction, *J. Chem. Phys.,* **137**(16), 1–6.

Barthel, E., 2008. Adhesive elastic contacts: JKR and more, *J. Phys. D: Appl. Phys.,* **41**(16) .

Baumberger, T. & Caroli, C., 2006. Solid friction from stick-slip down to pinning and aging, *Adv. Phys.,* **55**(3-4), 279–348.

Ben-Zion, Y. & Ampuero, J.P., 2009. Seismic radiation from regions sustaining material damage, *Geophys. J. Int.,* **178**(3), 1351–1356.

Berliner, S., 1906. Über das Verhalten des Gußeisens bei langsamen Belastungswechseln, *Ann. Phys., Lpz.,* **325**(8), 572–562.

Bocquet, L., Charlaix, E., Ciliberto, S. & Crassous, J., 1998. Moisture-induced ageing in granular media and the kinetics of capillary condensation, *Nature,* **396**(6713), 735–737.

Borri-Brunetto, M., Chiaia, B. & Ciavarella, M., 2001. Incipient sliding of rough surfaces in contact: a multiscale numerical analysis, *Comput. Methods Appl. Mech. Eng.,* **190**(46-47), 6053–6073.

Brenguier, F., Campillo, M., Hadziioannou, C., Shapiro, N.M., Nadeau, R.M. & Larose, E., 2008. Postseismic relaxation along the San Andreas fault at Parkfield from continuous seismological observations, *Science,* **321**(5895), 1478–1481.

Brenguier, F., Campillo, M., Takeda, T., Aoki, Y., Shapiro, N.M., Briand, X., Emoto, K. & Miyake, H., 2014. Mapping pressurized volcanic fluids from induced crustal seismic velocity drops, *Science,* **345**(6192), 80–82.

Broda, D., Staszewski, W.J., Martowicz, A., Uhl, T. & Silberschmidt, V.V., 2014. Modelling of nonlinear crack–wave interactions for damage detection based on ultrasound—a review, *J. Sound Vib.,* **333**(4), 1097–1118.

Brodsky, E.E. & van der Elst, N.J., 2014. The uses of dynamic earthquake triggering, *Annu. Rev. Earth Planet. Sci.,* **42**(1), 317–339.

Bureau, L., Baumberger, T. & Caroli, C., 2002. Rheological aging and rejuvenation in solid friction contacts, *Eur. Phys. J. E,* **8**(3), 331–337.

Capozza, R. & Urbakh, M., 2012. Static friction and the dynamics of interfacial rupture, *Phys. Rev. B,* **86**(8), 1–6.

Capozza, R., Barel, I. & Urbakh, M., 2013. Probing and tuning frictional aging at the nanoscale, *Sci. Rep.,* **3,** 3–8.

Chaves, E.J. & Schwartz, S.Y., 2016. Monitoring transient changes within overpressured regions of subduction zones using ambient seismic noise, *Sci. Adv.,* **2**(1).

Claytor, K.E., Koby, J.R. & Tencate, J.A., 2009. Limitations of Preisach theory: elastic aftereffect, congruence, and end point memory, *Geophys. Res. Lett.,* **36**(6), 1–4.

Delsanto, P. & Scalerandi, M., 2003. Modeling nonclassical nonlinearity, conditioning, and slow dynamics effects in mesoscopic elastic materials, *Phys. Rev. B,* **68**(6), 1–9.

Duncan, J. & Chang, C.-Y., 1970. Nonlinear analysis of stress and strain in soils, *J. Soil Mech. Found. Div.,* **96,** 1629–1653.

Eiras, J.N., Vu, Q.A., Lott, M., Payá, J., Garnier, V. & Payan, C., 2016. Dynamic acousto-elastic test using continuous probe wave and transient vibration to investigate material nonlinearity, *Ultrasonics,* **69,** 29–37.

Favrie, N., Lombard, B. & Payan, C., 2015. Fast and slow dynamics in a nonlinear elastic bar excited by longitudinal vibrations, *Wave Motion,* **56,** 221–238.

Frye, K.M. & Marone, C., 2002. Effect of humidity on granular friction at room temperature, *J. geophys. Res.,* **107**(B11), ETG 11–1-ETG 11-13.

Gassenmeier, M., Sens-Schönfelder, C., Eulenfeld, T., Bartsch, M., Victor, P., Tilmann, F. & Korn, M., 2016. Field observations of seismic velocity changes caused by shaking-induced damage and healing due to mesoscopic nonlinearity, *Geophys. J. Int.,* **204**(3), 1490–1502.

Gliozzi, A.S. & Scalerandi, M., 2014. Modeling dynamic acousto-elastic testing experiments: validation and perspectives, *J. acoust. Soc. Am.,* **136**(4), 1530–1541.

Goebel, T.H., Kwiatek, G., Becker, T.W., Brodsky, E.E. & Dresen, G., 2017. What allows seismic events to grow big?: insights from b-value and fault roughness analysis in laboratory stick-slip experiments, *Geology,* **45**(9), 815–818.

Gusev, V. & Tournat, V., 2005. Amplitude- and frequency-dependent nonlinearities in the presence of thermally-induced transitions in the Preisach model of acoustic hysteresis, *Phys. Rev. B,* **72**(5), 1–19.

Guyer, R. & Johnson, P.A., 2009. *Nonlinear Mesoscopic Elasticity: The Complex Behaviour of Rocks, Soil, Concrete,* Wiley .

Guyer, R., McCall, K. & Boitnott, G., 1995. Hysteresis, discrete memory, and nonlinear wave propagation in rock: a new paradigm, *Phys. Rev. Lett.,* **74**(17), 3491–3494.

Guyer, R.A. & Johnson, P.A., 1999. Nonlinear mesoscopic elasticity: evidence for a new class of materials, *Phys. Today,* 30–36.

Guyer, R.A., McCall, K.R., Boitnott, G., B, H.J.L. & Plona, T.J., 1997. Quantitative implementation of Preisach–Mayergoyz space to find static and dynamic elastic moduli in rock, *J. geophys. Res.,* **102,** 5281–5293.

Guyer, R.A., McCall, K.R. & Van Den Abeele, K., 1998. Slow elastic dynamics in a resonant bar of rock, *Geophys. Res. Lett.,* **25**(10), 1585–1588.

Hardin, B.O. & Drnevich, V.P., 1972. Shear modulus and damping in soils: design equations and curves, *Soil Mech. Found. Div.,* **98**(SM7), 667–692.

Hill, D.P. *et al.*, 1993. Seismicity remotely triggered by the magnitude 7.3 Landers, California, Earthquake, *Science,* **260,** 1617–1624.

Hilloulin, B., Legland, J.B., Lys, E., Abraham, O., Loukili, A., Grondin, F., Durand, O. & Tournat, V., 2016. Monitoring of autogenous crack healing in cementitious materials by the nonlinear modulation of ultrasonic coda waves, 3D microscopy and X-ray microtomography, *Constr. Build. Mater.,* **123,** 143–152.

Hobiger, M., Wegler, U., Shiomi, K. & Nakahara, H., 2014. Single-station cross-correlation analysis of ambient seismic noise : application to stations in the surroundings of the 2008 Iwate–Miyagi Nairiku earthquake, *Geophys. J. Int.,* **198**(1), 90–109.

Johnson, P. & Sutin, A., 2005. Slow dynamics and anomalous nonlinear fast dynamics in diverse solids, *J. acoust. Soc. Am.,* **117**(1), 124–130.

Johnson, P.A., Zinszner, B. & Rasolofosason, P.N., 1996. Resonance and elastic nonlinear phenomena in rock, *J. geophys. Res.,* **101**(96), 553–564.

King, M.S. & Paulsson, B.N.P., 1981. Acoustic velocities in heated block of granite subjected to uniaxial stress, *Geophys. Res. Lett.,* **8**(7), 699–702.

Landau, L., Lifshitz, E., Kosevich, A. & Pitaevskiĭ, L., 1986. *Theory of Elasticity, Course of theoretical physics,* Elsevier .

Larose, E. & Hall, S., 2009. Monitoring stress related velocity variation in concrete with a 2 x 10(-5) relative resolution using diffuse ultrasound, *J. acoust. Soc. Am.,* **125**(4), 1853–1856.

Lavrov, A., 2003. The Kaiser effect in rocks: principles and stress estimation techniques, *Int. J. Rock Mech. Min. Sci.,* **40**(2), 151–171.

Lesage, P., Reyes-Dávila, G. & Arámbula-Mendoza, R., 2014. Large tectonic earthquakes induce sharp temporary decreases in seismic velocity in Volcán de Colima, Mexico, *J. geophys. Res.,* 4360–4376.

Li, A., Liu, Y. & Szlufarska, I., 2014. Effects of interfacial bonding on friction and wear at silica/silica interfaces, *Tribol. Lett.,* **56**(3), 481–490.

Li, Q., Tullis, T.E., Goldsby, D. & Carpick, R.W., 2011. Frictional ageing from interfacial bonding and the origins of rate and state friction, *Nature,* **480**(7376), 233–236.

Li, X., Sens-Schönfelder, C. & Snieder, R., 2018. Nonlinear elasticity in resonance experiments, *Phys. Rev. B,* **97,** 1–9.

Lieou, C.K.C., Daub, E.G., Guyer, R.A. & Johnson, P.A., 2017. Nonlinear softening of unconsolidated granular earth materials, *J. geophys. Res.,* **122**(9), 6998–7008.

Liu, Y. & Szlufarska, I., 2012. Chemical origins of frictional aging, *Phys. Rev. Lett.,* **109**(18), 1–5.

Lott, M., Remillieux, M.C., Garnier, V., Le Bas, P.-Y., Ulrich, T.J. & Payan, C., 2017. Nonlinear elasticity in rocks: a comprehensive three-dimensional description, *Phys. Rev. Mater.,* **1**(2).

Lyakhovsky, V., Ben-Zion, Y. & Agnon, A., 1997. Distributed damage, faulting, and friction, *J. geophys. Res.,* **102**(B12), 27 635–27 649.

Lyakhovsky, V., Hamiel, Y., Ampuero, J.P. & Ben-zion, Y., 2009. Non-linear damage rheology and wave resonance in rocks, *Geophys. J. Int.,* **178**(2), 910–920.

Marc, O., Hovius, N., Meunier, P., Uchida, T. & Hayashi, S., 2015. Transient changes of landslide rates after earthquakes, *Geology,* **43**(10), 883–886.

Marone, C., 1998. Laboratory-derived friction laws and their application to seismic faulting, *Annu. Rev. Earth Planet. Sci.,* **26**(1), 643–696.

Mo, Y., Turner, K.T. & Szlufarska, I., 2009. Friction laws at the nanoscale, *Nature,* **457**(7233), 1116–1119.

Nagata, K., Nakatani, M. & Yoshida, S., 2008. Monitoring frictional strength with acoustic wave transmission, *Geophys. Res. Lett.,* **35**(6), 1–5.

Nishimura, T., 2017. Triggering of volcanic eruptions by large earthquakes, *Geophys. Res. Lett.,* **44**(15), 7750–7756.

Ostrovsky, L.A. & Johnson, P.A., 2001. Dynamic nonlinear elasticity in geomaterials, *Riv. Nuovo Cimento,* **24**(7), 1–46.

Pasqualini, D., Heitmann, K., TenCate, J.A., Habib, S., Higdon, D. & Johnson, P.A., 2007. Nonequilibrium and nonlinear dynamics in Berea and Fontainebleau sandstones: low-strain regime, *J. geophys. Res.,* **112**(1), 1–16.

Pecorari, C., 2015. Modeling the elasto-acoustic hysteretic nonlinearity of dry Berea sandstone, *Wave Motion,* **52,** 66–80.

Popov, V., 2010. *Contact Mechanics and Friction,* Springer.

Prandtl, L., 1928a. Ein Gedankenmodell zur kinetischen Theorie der festen Körper, *Z. Angew. Math. Mech.,* **8**(2), 85–106.

Remillieux, M.C., Ulrich, T.C., Goodman, H.E. & Ten Cate, J.A., 2017. Propagation of a finite-amplitude elastic pulse in a bar of Berea sandstone: a detailed look at the mechanisms of classical nonlinearity, hysteresis, and nonequilibrium dynamics, *J. geophys. Res.,* **122,** 8892–8909.

Renaud, G., Le Bas, P.Y. & Johnson, P.A., 2012. Revealing highly complex elastic nonlinear (anelastic) behavior of Earth materials applying a new probe: dynamic acoustoelastic testing, *J. geophys. Res.,* **117,** 1–17.

Renaud, G., Rivière, J., Le Bas, P.Y. & Johnson, P.A., 2013. Hysteretic nonlinear elasticity of Berea sandstone at low-vibrational strain revealed by dynamic acousto-elastic testing, *Geophys. Res. Lett.,* **40**(4), 715–719.

Renaud, G., Rivière, J., Larmat, C., Rutledge, J., Lee, R., Guyer, R., Stokoe, K. & Johnson, P., 2014. In situ characterization of shallow elastic nonlinear parameters with Dynamic Acoustoelastic Testing, *J. geophys. Res.,* **119,** 6907–6923.

Rice, J.R., Lapusta, N. & Ranjith, K., 2001. Rate and state dependent friction and the stability of sliding between elastically deformable solids, *J. Mech. Phys. Solids,* **49**(9), 1865–1898.

Richter, T., Sens-Schönfelder, C., Kind, R. & Asch, G., 2014. Comprehensive observation and modeling of earthquake and temperature-related seismic velocity changes in northern Chile with passive image interferometry, *J. geophys. Res.,* **119,** 4747–4765.

Rivière, J., Renaud, G., Guyer, R.A. & Johnson, P., 2013. Pump and probe waves in dynamic acousto-elasticity: comprehensive description and comparison with nonlinear elastic theories, *J. Appl. Phys.,* **114**(5), 1–19.

Rivière, J., Remillieux, M.C., Ohara, Y., Anderson, B.E., Haupert, S., Ulrich, T.J. & Johnson, P.A., 2014. Dynamic acousto-elasticity in a fatigue-cracked sample, *J. Nondestruct. Eval.,* **33**(2), 216–225.

Rivière, J., Shokouhi, P., Guyer, R.A. & Johnson, P.A., 2015. A set of measures for the systematic classification of the nonlinear elastic behavior of disparate rocks, *J. geophys. Res.,* **120,** 1–18.

Rivière, J., Pimienta, L., Scuderi, M., Candela, T., Shokouhi, P., Fortin, J., Schubnel, A., Marone, C. & Johnson, P.A., 2016. Frequency, pressure, and

strain dependence of nonlinear elasticity in Berea Sandstone, *Geophys. Res. Lett.,* **43**(7), 3226–3236.

Scholz, C.H., 1998. Earthquakes and friction laws, *Nature,* **391**(6662), 37–42.

Sens-Schönfelder, C. & Wegler, U., 2011. Passive image interferometry for monitoring crustal changes with ambient seismic noise, *C. R. Geosci.,* **343,** 639–651.

Shapiro, S., 2003. Elastic piezosensitivity of porous and fractured rocks, *Geophysics,* **68**(2), 482–486.

Shokouhi, P., Rivière, J., Guyer, R.A., Johnson, P.A., Shokouhi, P., Rivie, J., Guyer, R.A. & Johnson, P.A., 2017. Slow dynamics of consolidated granular systems: multi-scale relaxation, **111,** 2–5.

Snieder, R., Sens-Schönfelder, C. & Wu, R., 2017. The time dependence of rock healing as a universal relaxation process: a tutorial, *Geophys. J. Int.,* **208**(2), 1–9.

TenCate, J., Smith, E. & Guyer, R., 2000. Universal slow dynamics in granular solids, *Phys. Rev. Lett.,* **85**(5), 1020–1023.

TenCate, J.a., 2011. Slow dynamics of earth materials: an experimental overview, *Pure appl. Geophys.,* **168**(12), 2211–2219.

TenCate, J.A., Pasqualini, D., Habib, S., Heitmann, K., Higdon, D. & Johnson, P.A., 2004. Nonlinear and nonequilibrium dynamics in geomaterials, *Phys. Rev. Lett.,* **93**(6), 4–7.

TenCate, J.A., Malcolm, A.E., Feng, X. & Fehler, M.C., 2016. The effect of crack orientation on the nonlinear interaction of a *P* wave with an *S* wave, *Geophys. Res. Lett.,* **43,** 6146–6152.

Tian, K., Gosvami, N.N., Goldsby, D.L., Liu, Y., Szlufarska, I. & Carpick, R.W., 2017. Load and time dependence of interfacial chemical bond-induced friction at the nanoscale, *Phys. Rev. Lett.,* **118,** 1–6.

Tomlinson, G., 1929. CVI. A molecular theory of friction, *London Edinburgh Dublin Phil. Mag. J. Sci.,* **7**(46), 905–939.

Trarieux, C., Callé, S., Moreschi, H., Renaud, G. & Defontaine, M., 2014. Modeling nonlinear viscoelasticity in dynamic acoustoelasticity , *Appl. Phys. Lett.,* **105,** 1–5.

Tremblay, N., Larose, E. & Rossetto, V., 2010. Probing slow dynamics of consolidated granular multicomposite materials by diffuse acoustic wave spectroscopy, *J. acoust. Soc. Am.,* **3**(127), 1–6.

Vakhnenko, O.O., Vakhnenko, V.O., Shankland, T.J. & TenCate, J.A., 2006. Soft-ratchet modeling of slow dynamics in the nonlinear resonant response of sedimentary rocks, *AIP Conf. Proc.,* **838,** 120–123.

Vanaverbeke, S. & Abeele, K.V.D., 2007. Two-dimensional modeling of wave propagation in materials with hysteretic nonlinearity, *J. acoust. Soc. Am.,* **122**(1), 58–72.

Vanorio, T., 2015. Recent advances in time-lapse, laboratory rock physics for the characterization and monitoring of fluid-rock interactions, *Geophysics,* **80**(2), WA49–WA59.

Vanorio, T. & Kanitpanyacharoen, W., 2015. Rock physics of fibrous rocks akin to Roman concrete explains uplifts at Campi Flegrei Caldera, *Science,* **349**(6248), 617–621.

Watt, S.F.L., Pyle, D.M. & Mather, T.A., 2009. The influence of great earthquakes on volcanic eruption rate along the Chilean subduction zone, *Earth planet. Sci. Lett.,* **277**(3-4), 399–407.

Wegler, U. & Sens-Schönfelder, C., 2007. Fault zone monitoring with passive image interferometry, *Geophys. J. Int.,* **168**(3), 1029–1033.

Wiktor, V. & Jonkers, H.M., 2011. Quantification of crack-healing in novel bacteria-based self-healing concrete, *Cem. Concr. Compos.,* **33**(7), 763–770.

Woodhouse, J., Putelat, T. & McKay, A., 2015. Are there reliable constitutive laws for dynamic friction?, *Phil. Trans. R. Soc. Lond., A,* **373**(2051).

Zaitsev, V.Y., Nazarov, V.E., Tournat, V., Gusev, V.E. & Castagnède, B., 2005. Luxemburg-Gorky effect in a granular medium: probing perturbations of the material state via cross-modulation of elastic waves, *Europhys. Lett.,* **70**(5), 607–613.

Zaitsev, V.Y., Gusev, V.E., Tournat, V. & Richard, P., 2014. Slow relaxation and aging phenomena at the nanoscale in granular materials, *Phys. Rev. Lett.,* **112**.